Characterizing errors in parameter estimation by local measurements

Riddhi Ghosh [1,*] Alexei Gilchrist [1] and Daniel Burgarth [2]
[1]*School of Mathematical and Physical Sciences, Macquarie University, Sydney, Australia*
[2]*Friedrich-Alexander-Universität Erlangen-Nürnberg, Erlangen, Germany*

(Received 18 June 2025; accepted 2 March 2026; published 5 May 2026)

The indirect estimation of couplings in quantum dynamics relies on the measurement of the spectrum and the overlap of eigenvectors with some reference states. These data can be obtained by local measurements on some sites and eliminate the need for full Hamiltonian tomography. For a one-dimensional (1D) chain, access to only one edge site is sufficient to compute all the couplings between the adjacent sites, and consequently to reconstruct the full Hamiltonian. However, its robustness in the presence of perturbations remains a critical question, particularly when sites interact with other lattice sites beyond nearest neighbors. Our work studies the applicability of schemes designed for 1D chains to topologies with interactions beyond nearest neighbor. We treat interactions between the next-nearest sites as perturbation of strength ε and show that the error in estimation of couplings scales linearly with ε in the presence of such interactions. Further, we show that, on average, the existence of couplings between sites beyond the next-nearest neighbor results in higher error. We also study the length of the chain that can be estimated (up to a fixed precision) as a function of ε, in the presence of next-nearest-neighbor interactions. Typically, for weak interactions, chains of 30 sites can be estimated within reasonable error. Thus, we study the robustness of estimation scheme designed for a 1D chain when exposed to such multisite perturbations, offering valuable insights into its applicability and limitations.

DOI: 10.1103/4czy-q998

I. INTRODUCTION

Hamiltonian tomography and parameter estimation are important for the design of quantum devices for quantum technologies such as quantum computation, communication, and metrology. Since these quantum devices need to be carefully isolated to prevent unwanted interactions and noise, they are often difficult to probe, and characterization methods are frequently constrained. Various methods for estimating the parameters of the Hamiltonian governing the system have been explored.

Such characterization schemes span from performing full informationally complete tomography to the application of machine learning algorithms on restricted data. Several studies leverage maximum likelihood estimation for deducing the Hamiltonians based on local measurements [1–7]. Notably, maximum likelihood estimation can be merged with matrix product operators to provide a scalable estimation method [8]. Methods for quantum-state or process tomography using linear regression methods have also been studied [9,10]. In Refs. [11–13], the authors present an algorithm for Hamiltonian learning using copies of the Gibbs state. Other approaches involve optimal measurement strategies for extracting maximum information from measurement and methods from sensing and metrology [14–17].

A notable approach proposed in Ref. [18] is the method of indirect estimation of couplings through local measurements conducted on a subset of the sites within a specified lattice. This method relies on the precise determination of the spectrum and the overlap of the eigenvectors with designated reference states; these represent local probes. For example, in a one-dimensional system with N sites, complete knowledge of the spectrum $\{e_k\}$, and the overlap between each eigenvector and a reference state, say $|1\rangle$ corresponding to a local probe measured at one end of the chain (quantified by $|\langle 1|e_k\rangle|^2$) is sufficient to estimate all the couplings between the sites. While the spectrum constitutes a global property of the entire chain, it can be effectively extracted from the free-induction decay (FID) signal obtained by initializing and measuring a single excitation at one end of the chain [18]. Specifically, the Fourier transform of the FID reveals both the energy eigenvalues and the squared overlaps $|\langle 1|e_k\rangle|^2$, thereby providing the required spectral information through local measurements. Alternatively, one may measure only the spectra, but in the presence of a local perturbation [19]. For a one-dimensional chain with only nearest-neighbor interaction, performing measurement at one end of the chain is sufficient; this will be discussed in more detail in Sec. II. This approach significantly reduces the resources that would otherwise be needed for complete state tomography, but potentially comes at a price of lower precision.

The robustness of this scheme has been studied in the context of a one-dimensional linear topology. The impact of errors occurring during measurement and experimental implementation, encompassing factors such as insufficient resolution, constrained signal-to-noise ratio, and various other experimental and instrumental inaccuracies, has been explored in

*Contact author: riddhighosh22@gmail.com

Published by the American Physical Society under the terms of the Creative Commons Attribution 4.0 International license. Further distribution of this work must maintain attribution to the author(s) and the published article's title, journal citation, and DOI.

Ref. [20]. The study examines the effect of imprecise measurements that lead to partial loss of information due to broadening of the spectral peaks. To address this, the recursive relations introduced in Refs. [18,19] were modified to add a correction term designed to accommodate missing or insufficient experimental data [20]. The scheme has been shown to be robust when this correction term is introduced.

Subsequent investigations have expanded on the original work in Ref. [18], demonstrating the applicability of the algorithm to arbitrary networks, where measurements are carried out at multiple local sites [21]. Estimation of couplings for networks with interactions beyond the nearest neighbor involves the concept zero forcing [21–23]. Zero forcing establishes a set of rules that are useful to identify the set of vertices that are sufficient for indirect estimation of couplings between all the sites. This will be discussed in detail in Sec. II. It is noteworthy that the concept of zero forcing is intimately related with the controllability of these networks [22].

Experimentally, the interplay between estimation and controllability has been exploited for quantum-state tomography using nitrogen-vacancy centers in diamond coupled to a nuclear spin in Ref. [24]. The study shows that when a system is controllable by a driven single qubit, then a local random pulse is sufficient for a complete quantum-state tomography. Another experimental implementations of estimation despite restricted access to the system is presented in Ref. [25], where quantum system identification is achieved by analyzing free induction decay signals. The experiment is implemented using liquid nuclear magnetic resonance quantum information processor and is based on the measurement of time traces of a restricted subsystem [26].

It is important to acknowledge that a single site may exhibit interactions with multiple sites that extend beyond its immediate neighbors. Indeed, in the usual experimental setup, most sites within the system interact with each other, typically with a decreasing interaction strength as the distance between them increases. Sometimes, interactions beyond nearest neighbor are sufficiently weak and can be ignored. In this paper, we study the robustness of the protocol in experimental configurations where such long-range interactions might be relevant. Our primary focus centers on a scenario in which the presence of such couplings beyond nearest neighbors is unknown. Consequently, we implement the protocol with the assumption of nearest-neighbor interactions and seek to determine whether the resulting errors have any significant impact on the estimation of the coupling strength.

In Sec. II, we start with a description of the scheme employed for the indirect estimation of couplings for nearest-neighbor interactions. We provide a concise overview of the zero-forcing conditions [22,23], which serve as the foundation for understanding how the original scheme could be adapted when interactions are known to extend beyond nearest neighbor. Furthermore, we present an extension of the estimation protocol tailored to accommodate next-nearest-neighbor couplings. Our results are organized into three distinct subsections. In Sec. III A, we derive an analytical error bound for estimation up to the second coupling and formulate an ansatz capturing the behavior for $n \geqslant 3$, where the nth term represents coupling between n and $n+1$ sites. This is followed by Sec. III B, where we investigate the critical length, i.e., the number of couplings that can be estimated up to a fixed precision, as a function of the strength of perturbation. Finally, in Sec. III C, we expand the study to systems with interactions beyond the next-nearest neighbors.

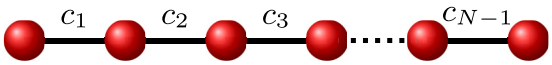


FIG. 1. Topology corresponding to the Hamiltonian with nearest-neighbor interactions. The black lines denote the couplings.

II. MATHEMATICAL FRAMEWORK

Zero forcing is a concept closely linked to the controllability of a system with a known topology. The connection between zero forcing and quantum system identification and parameter estimation has been well established in previous research [27]. Consider a simple graph where the vertices may be white or blue, and an iterative process where a blue vertex in a graph turns a neighbor blue if and only if it is the only white neighbor of that vertex; the blue vertices remain blue. The iterative process is continued until no further change happens. A zero-forcing set is a subset of vertices in a graph that turns all the other vertices blue.

In the context of tight-binding models or spin chains, within first excitation sector, the system Hamiltonian can be represented as a hopping Hamiltonian on a graph, where the sites correspond to the vertices and the couplings to the edges. The size of a minimum zero-forcing set of a given graph is called the zero-forcing number and is an upper bound for the degeneracy of the Hamiltonian governing the system [28]. The minimum zero-forcing set also gives the number of sites that are sufficient to perform local measurements on, in order to estimate the couplings in a given network by applying the estimation scheme [18,19].

A simple example illustrating the applicability of zero forcing is that of a one-dimensional chain with N sites. We consider a Hilbert space $\mathcal{H}$ of dimension N equipped with the orthonormal basis vectors $\{|1\rangle, |2\rangle, \ldots, |N\rangle\}$. A hopping Hamiltonian within this space can be written as $H_C = \sum_{n=1}^{N-1} c_n(|n\rangle\langle n+1| + |n+1\rangle\langle n|)$, where the coupling strength between the nth and $(n+1)$th sites is c_n, $1 \leqslant n \leqslant N-1$ (see Fig. 1). Here, we choose c_n as real and positive. This choice incurs no loss of generality in the one-dimensional case—Any complex value $c_n' = |c_n|e^{i\theta_n}$ can be mapped to a real, positive value by a local gauge transformation, specifically by applying site-dependent phase shifts $|n'\rangle \to e^{i\theta_n}|n\rangle$. Such transformations do not affect the underlying physics and any complex phase can be absorbed in a choice of basis [19].

Knowing the spectrum of H_C given by $\{e_k\}$ and the overlap of the first site with a reference state, i.e., $\langle 1|e_k\rangle$, we can determine that $c_1^2 = \sum_{k=1}^{N} |e_k\langle 1|e_k\rangle|^2$ and $\langle 2|e_k\rangle = e_k\langle 1|e_k\rangle/c_1$. The required spectral data can be obtained from local dynamical measurements. If an excitation is initialized on site $|1\rangle$, the return amplitude

$$f(t) = \langle 1|\, e^{-iHt}\, |1\rangle \tag{1}$$

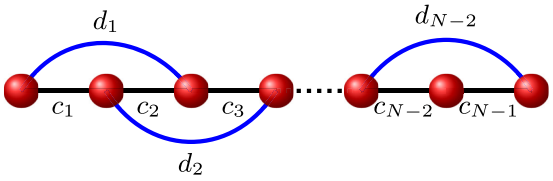


FIG. 2. Topology corresponding to the Hamiltonian with nearest- and next-nearest-neighbor interactions. The black lines denote the nearest-neighbor couplings and the blue lines denote the next-nearest-neighbor couplings.

can be recorded as a function of time. Its Fourier transform yields

$$F(\omega) = \sum_k |\langle 1|e_k^2\rangle| \delta(\omega - e_k), \tag{2}$$

where the position of the peaks correspond to the eigenvalues e_k, while the heights of the peaks give the amplitudes $|\langle 1|e_k^2\rangle|^2$. Thus, both the spectrum and the local projections of eigenvectors can be extracted from the FID signal measured at a single site.

The coupling constants for $n \geqslant 2$ can be calculated using the following recursive formulas [18] (see Appendix A for derivation):

$$c_n = \sqrt{\sum_{k=1}^{N} |e_k \langle n|e_k\rangle - c_{n-1}\langle n-1|e_k\rangle|^2}, \tag{3}$$

$$\langle n+1|e_k\rangle = \frac{e_k\langle n|e_k\rangle - c_{n-1}\langle n-1|e_k\rangle}{c_n}. \tag{4}$$

Zero forcing also indicates that in the presence of next-nearest-neighbor interactions, local measurements on more than one site may be necessary to obtain all the couplings.

We now treat the next-nearest-neighbor term as a perturbation to the original Hamiltonian H_C. We use d_l to represent the coupling between the lth and $(l+2)$th site $(1 \leqslant l \leqslant N-2)$; in accordance with c_n and for the sake of simplicity, we choose d_l also to be real and positive. The magnitudes of both c_n and d_l are of the same order. The interaction strength of the nearest-neighbor sites is on the order of c_n, while that of next-nearest neighbor is controlled by the strength of perturbation ε; i.e., the coupling is proportional to ϵd_l. The modified Hamiltonian is $H^\epsilon = H_C + \epsilon H_D$, where $H_D = \sum_{l=1}^{N-2} d_l(|l\rangle\langle l+2| + |l+2\rangle\langle l|)$ and $0 \leqslant \epsilon \leqslant 1$ is the strength of perturbation. The topology corresponding to H^ϵ is shown in Fig. 2.

The spectrum of the Hamiltonian H^ϵ is denoted as $\{e_k^\epsilon\}$ and the eigenvectors are $\{|e_k^\epsilon\rangle\}$, $k = 1, \ldots, N$. Building upon the calculations in the previous case, it becomes evident that $c_1 = \sum_{k=1}^{N} e_k^\epsilon \langle 1|e_k^\epsilon\rangle\langle e_k^\epsilon|2\rangle$. Thus, in order to compute c_1 using this estimation scheme, it is sufficient to have the knowledge of $\{e_k^\epsilon\}$ and the coefficients $\langle 1|e_k^\epsilon\rangle$ and $\langle 2|e_k^\epsilon\rangle$. Furthermore, we observe that $\epsilon^2 d_1^2 = \sum_{k=1}^{N} |e_k^\epsilon\langle 1|e_k^\epsilon\rangle - c_1\langle 2|e_k^\epsilon\rangle|^2$ and $\langle 3|e_k^\epsilon\rangle = (e_k^\epsilon\langle 1|e_k^\epsilon\rangle - c_1\langle 2|e_k^\epsilon\rangle)/\epsilon d_1$. By following this methodology, it is possible to compute all the coupling coefficients c_n's and d_n's for $n \geqslant 2$ using the recursive relation stated below:

$$c_n = \sum_{k=1}^{N} e_k^\epsilon \langle n|e_k^\epsilon\rangle\langle e_k^\epsilon|n+1\rangle, \tag{5}$$

$$\epsilon^2 d_n^2 = \sum_{k=1}^{N} \left|e_k^\epsilon\langle n|e_k^\epsilon\rangle - c_{n-1}\langle n-1|e_k^\epsilon\rangle - c_n\langle n+1|e_k^\epsilon\rangle\right|^2, \tag{6}$$

$$\langle n+2|e_k^\epsilon\rangle = \frac{e_k^\epsilon\langle n|e_k^\epsilon\rangle - c_{n-1}\langle n-1|e_k^\epsilon\rangle - c_n\langle n+1|e_k^\epsilon\rangle}{\epsilon d_n}. \tag{7}$$

The spectral decomposition of the dynamics of the system can be accessed via the Fourier transform of the FID, which provides the magnitudes of overlaps $|\langle 1|e_k^\epsilon\rangle|^2$ and $|\langle 2|e_k^\epsilon\rangle|^2$ onto the energy eigenstates [19]. While this provides the modulus of the overlaps, full reconstruction of the complex coefficients $\langle 1|e_k^\epsilon\rangle$ and $\langle 2|e_k^\epsilon\rangle$ requires knowledge of their relative phases. These phases are not accessible through FID alone but can be inferred from coherent transport measurements. As demonstrated in Ref. [21], by analyzing the time-resolved propagation of local excitations, one can extract the phase information necessary to reconstruct the full complex structure of the eigenstate projections. Consequently, we establish that for the topological network described by the Hamiltonian H^ϵ, measuring two specific sites is sufficient to obtain information regarding all the couplings and therefore the Hamiltonian. This observation aligns with the zero-forcing condition.

However, if one is unaware of the next-nearest-neighbor couplings and the estimation protocol designed for nearest-neighbor interactions is applied regardless, the extended interactions effectively introduce an error in the estimated values of the couplings. This is the setup that we consider now.

III. RESULTS

In the previous section, we realized that for a chain with next-nearest-neighbor interaction, the values of $\{e_k^\epsilon\}$, $\langle 1|e_k\rangle$, and $\langle 2|e_k\rangle$ are sufficient in order to effectively deduce all the coupling constants. In the instances where the knowledge of $\langle 2|e_k\rangle$ is lacking or where one is unaware of next-nearest-neighbor couplings, one can still try to compute the nearest-neighbor couplings by applying the estimation scheme for a chain with nearest-neighbor interaction only. However, the coupling constants estimated using this methodology may exhibit some degree of deviation from their true values. Our aim is to find out how the magnitude of this discrepancy depends on the strength of the perturbation ϵ.

A. Upper bound of error in estimation for up to $N = 30$

Considering that we employ the estimation scheme for nearest-neighbor coupling although our system is characterized by next-nearest-neighbor interaction, the calculated coupling coefficients exhibit inaccuracies; we denote these couplings as c_n^ϵ. In the absence of perturbation, i.e., when $\epsilon = 0$, $c_n^\epsilon = c_n$. We quantify the error at site n, resulting from the omission of next-nearest-neighbor couplings as $\Delta_n = \sqrt{|(c_n^\epsilon)^2 - c_n^2|}$.

Using the formulas presented in Sec. II, we can derive the expression $(c_1^\epsilon)^2 = \sum_{k=1}^{N}(e_k^\epsilon)^2|\langle 1|e_k^\epsilon\rangle|^2$ (see Appendix A). Furthermore, $\langle 1|(H^\epsilon)^2|1\rangle = \sum_{k=1}^{N}(e_k^\epsilon)^2|\langle 1|e_k^\epsilon\rangle|^2 = c_1^2 + \epsilon^2 d_1^2$. Consequently, the square of the error in calculating the coupling constant between the first and second sites is (see Appendix B)

$$\Delta_1 = \sqrt{\left|\left(c_1^\epsilon\right)^2 - c_1^2\right|} = \epsilon d_1, \tag{8}$$

as is expected from perturbation theory. Now, we use the recursive relations for nearest-neighbor interaction outlined in Sec. II to define the following terms, for $n \geqslant 2$,

$$\left(c_n^{\epsilon}\right)^2 := \sum_{k=1}^{N} \left| e_k^{\epsilon} \langle n|e_k\rangle_{\varepsilon} - c_{n-1}^{\epsilon} \langle n-1|e_k\rangle_{\varepsilon} \right|^2, \tag{9}$$

$$\langle n+1|e_k\rangle_{\varepsilon} := \frac{e_k^{\epsilon} \langle n|e_k\rangle_{\varepsilon} - c_{n-1}^{\epsilon} \langle n-1|e_k\rangle_{\varepsilon}}{c_n^{\epsilon}}. \tag{10}$$

It is essential to note that the subscript ε signifies that the term $\langle n|e_k\rangle_{\varepsilon}$ is not the overlap of $|n\rangle$ with the eigenvectors of the system, i.e., $\langle n|e_k^{\epsilon}\rangle \neq \langle n|e_k\rangle_{\varepsilon}$. Rather, it is the *estimated* overlap—the numerical value that we calculate from the estimation protocol, including an approximation error. We obtain

$$\Delta_2 = \epsilon\left(d_2 + \frac{d_1 c_3}{c_1}\right) + \mathcal{O}(\epsilon^2). \tag{11}$$

Since ϵ is small, we ignore the higher-order terms from $\mathcal{O}(\epsilon^2)$ and conclude that Δ_2 also scales with ϵ. Since the additional couplings are treated as perturbation, one expects errors on the order of ϵ. While this scaling is evident for the first two terms (Δ_1 and Δ_2), obtaining closed-form expressions for higher n becomes analytically intractable. The relevant quantity is not just the order of the error, but the coefficient in front of ϵ, and in particular how it scales with the site n. We therefore introduce a heuristic ansatz to approximate the overall growth of the error with n,

$$\Delta_n \leqslant n^p \epsilon(\max(d_k)), \tag{12}$$

where p is an empirically chosen exponent that provides the best fit to the numerical data. This ansatz is not derived analytically but was found to accurately describe the observed scaling. A numerical study shows that for up to $N = 30$, we can choose $p = 7/6$ to get a fairly tight upper bound for the error in estimation, as shown in Fig. 3. It serves as a convenient empirical upper bound consistent with the linear ϵ dependence obtained from perturbation theory.

Figure 3 illustrates the behavior of estimation error when the ideal nearest-neighbor model is perturbed by weak next-nearest-neighbor couplings. The black points show the average deviation from the actual coupling strength, while the red points indicate the empirical upper bound given in Eq. (12). The gradual increase in the error reflects the cumulative propagation of perturbative effects through the recursive estimation scheme. Importantly, the error remains small, demonstrating the robustness of the method.

For each simulation, c_n's and d_n's were chosen independently from uniform distributions centered at unity with a relative variation of 2.5%. Therefore, both $c_n, d_n \in [0.95, 1.05]$. The result shown in Fig. 3 represent averages over 1000 independent random realizations of these parameters.

It should also be noted here that the small drop observed in the error at the last site (in Fig. 3) arises from a finite-size boundary effect in the recursion procedure. At the edge of the chain, only one coupling is to be estimated at instead of two; this might make the error slightly lower. Increasing the chain size confirms this interpretation—for example, when $N = 40$, the site corresponding to $n = 29$ no longer shows a drop.

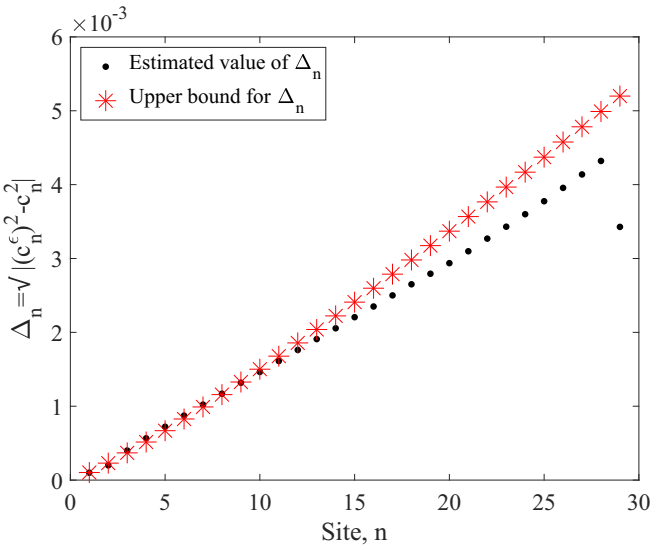


FIG. 3. The error Δ_n in estimation of the coupling constants in the presence of next-nearest-neighbor interaction. Each Δ_n is the average over 1000 randomly chosen Hamiltonians; the Hamiltonians are constructed with c_n and d_n randomly chosen from a uniform distribution lying in [0.95, 1.05]. The upper bound is given by $n^{\frac{7}{6}}\epsilon(\max(d_k))$, which is valid for up to $N = 30$. Here, $\epsilon = 10^{-4}$. Note: The last point ($n = N - 1$) shows a small drop due to a boundary effect in the recursion.

B. Critical length

It is evident from Fig. 3 that the error in the estimated value increases along the chain. Couplings can be estimated with reasonable accuracy up to a certain length that depends on the value of ϵ. In this context, we introduce the concept of *critical length*, L_C, which characterizes the segment of the chain (quantified by the number of coupling constants) that can be estimated within a predetermined margin of error, for a chain of length N. The behavior of L_C is extracted from exact numerical simulations. Figure 4 shows the variation of L_C with strength of perturbation ϵ, revealing a clear trend—as ϵ increases, the portion of the chain that remains accurately estimable decreases. By construction, in the absence of perturbation ($\epsilon = 0$), the estimation protocol exactly recovers all coupling, i.e., $L_C = N$, irrespective of the chain length.

The feasibility of the estimation algorithm becomes evident when applied to scenarios involving relatively minor perturbations, typically up to the magnitude of 10^{-3}. Many experimental setups feature considerably fewer than 50 sites. For instance, in the study presented in Ref. [29], a configuration consisting of 42 trapped ions is employed to investigate system dynamics with local observations. The estimation algorithm should perform well with such system sizes.

C. Generalization to interactions beyond next-nearest neighbor

We now consider scenarios where the system exhibits interactions beyond nearest neighbor. For a chain size of $N = 20$, we choose two distinct graphs where the interactions occur between 18 specific pairs of sites and compare the estimation errors with the case where next-nearest-neighbor interactions are present. In each case, the system also includes

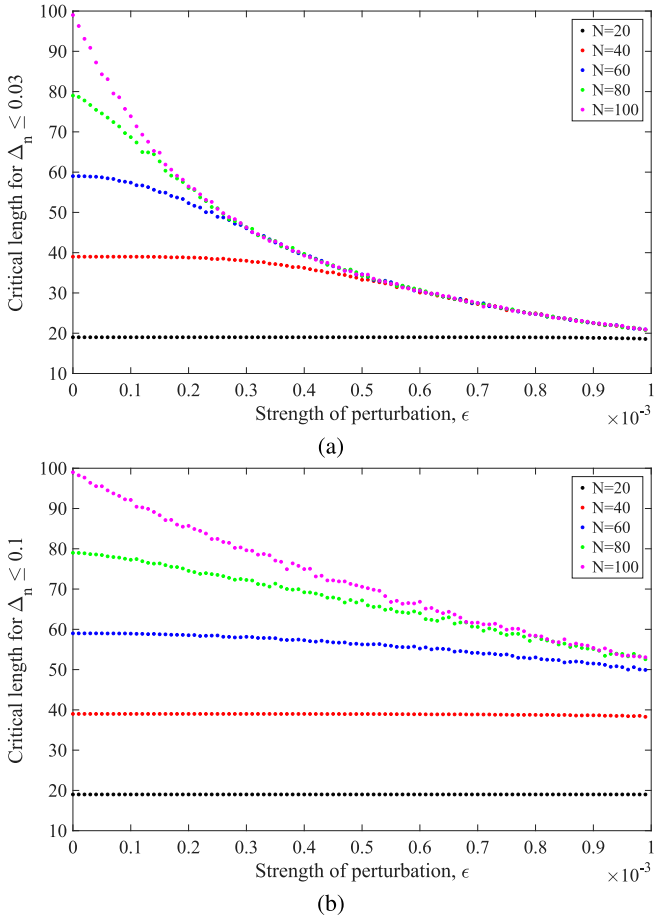


FIG. 4. The variation of the critical length L_C with the strength of perturbation ϵ, up to a precision of (a) 0.03 and (b) 0.1, for different lengths of chain N. The Hamiltonians are constructed with c_n and d_n randomly chosen from a uniform distribution lying in [0.95, 1.05]. For $\epsilon = 0$, the critical length $L_C = N$; all the couplings can be estimated for any N when $\varepsilon = 0$.

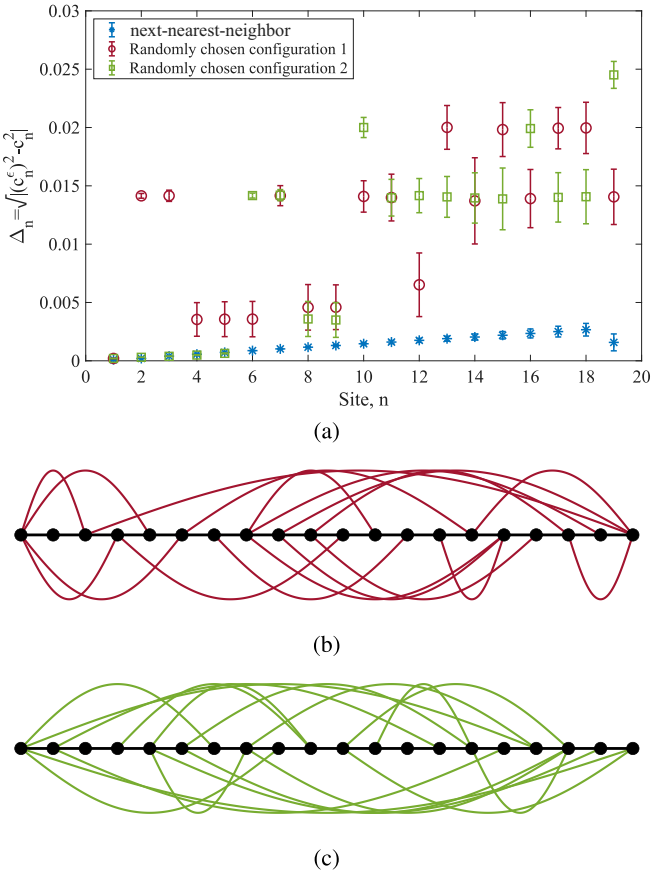


FIG. 5. (a) The average estimation error as a function of site n for three different adjacency profiles, for a chain of size $N = 20$. Each point is an average of 1000 instances of the Hamiltonian. The blue points correspond to the next-nearest-neighbor interactions. The error bars denote the standard deviation over all the random realizations. The overlap between green and blue points is expected, as these configurations yield similar average errors. The interaction structures of the chains corresponding to the red and green points, respectively, are shown in panels (b) and (c). Both cases include long-range interactions beyond next-nearest neighbor.

nearest-neighbor couplings. The strength of perturbation is fixed at $\varepsilon = 10^{-4}$ in each of these three different cases.

For each graph, we generate 1000 random instances of coupling strengths—c_n and d_n, sampled independently for each realization. The estimation error is then averaged over these 1000 cases to obtain an overall trend. Figure 5 shows the average estimation error for the three cases, along with the corresponding graphs. Here, we examine the effect of perturbations arising from non-nearest-neighbor couplings. The different sets of points correspond to configurations with the same number of additional couplings but at increasing spatial separations. This approach isolates the influence of interaction distance on estimation accuracy. Simply extending the interaction range would introduce only a few such links in a finite chain, providing insufficient statistics for meaningful averaging. By keeping the number of added couplings constant while varying their distance, we can compare the impact of perturbations on equal footing across different topologies.

On average, the system with next-nearest-neighbor interactions consistently exhibit lower error. While individual realizations in the other two cases can occasionally outperform the next-nearest-neighbor setup, the overall trend is clear. Additionally, the standard deviation in error is significantly smaller in the next-nearest-neighbor case, indicating more robust and predictable estimation performance.

Now, we look at a different setup where we randomly choose the adjacency structure as well as the interaction strengths. Figure 6 presents the behavior of critical length L_C averaged over 1000 random adjacency configurations. Each instance involves a different realization of the couplings along with randomly chosen set of interacting sites beyond nearest neighbors. We observed from Fig. 5 that the estimation algorithm performs worse in the presence of couplings beyond next-nearest neighbor. Consistent with the error trends, the next-nearest-neighbor case shows higher average L_C, whereas systems with randomly placed interactions tend to result in shorter critical lengths.

These results suggest that systems with structured extended couplings—such as next-nearest-neighbor interactions—not only are more amenable to parameter estimation but also

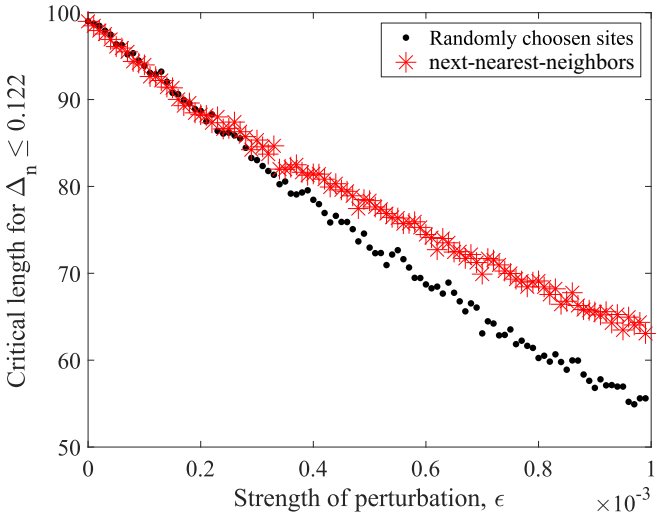


FIG. 6. The variation of the critical length L_C with the strength of perturbation ϵ, up to a precision of 0.122. The red star correspond to the L_C for next-nearest-neighbor interaction; the black dots represent the cases where the sites that are interaction are chosen at random. Each star/dot is an average of 1000 random instances of the Hamiltonian. The Hamiltonians are constructed with c_n and d_n randomly chosen from a uniform distribution lying in [0.95, 1.05].

exhibit lower variance. In contrast, the presence of arbitrarily placed couplings introduces greater uncertainty and leads to higher average error, even when the total number and strength of interactions remain fixed.

IV. CONCLUSION

Our study sheds light on the importance of the type and arrangement of couplings. Investigating coupling strength holds practical importance in experimental settings, as it informs the selection of appropriate pulse types for experiments. We highlight the significance of the system's structural information. While the loss of physical information can be mitigated through modifications to the original scheme [20], structural information plays a stronger and crucial role. A comprehensive understanding of the system's topology enables meaningful approximations and guides the adaptation of estimation schemes to realistic scenarios.

It is also conceivable that a similar extension could be achieved to unperturbed two- or three-dimensional scenarios. We have analyzed the estimation errors in a linear chain when perturbations effectively embed it into planar or spatial layouts. In the presence of perturbations, a network originally

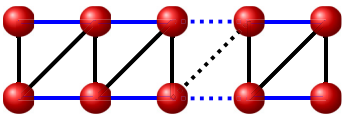


FIG. 7. Topology corresponding to the Hamiltonian for system exhibiting nearest- and next-nearest-neighbor interactions. This is a two-dimensional representation of the topology shown in Fig. 2. The black and blue lines denote nearest- and next-nearest-neighbor couplings, respectively.

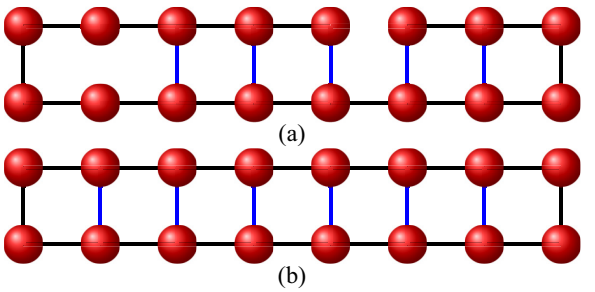


FIG. 8. Topology of qubits in IBM (a) QX3 and (b) QX5 architectures. Black and blue lines represent nearest and beyond nearest-neighbor interactions, respectively.

confined to two/three dimensions would likely introduce additional errors due to incomplete structural information. This is somewhat evident in Fig. 5, which demonstrates that the error is minimal when only next-nearest-neighbor couplings are present. However, when interactions occur between random pairs of sites, the error increases significantly.

It is worth observing that the one-dimensional topological structure associated with the couplings defined by the Hamiltonian featuring next-nearest-neighbor interactions (Fig. 2) can be equivalently represented as a two-dimensional system, as shown in Fig. 7. This transformation does not alter the underlying connectivity, but instead embeds the system in a higher-dimensional space where the interaction graph becomes locally simpler.

Such two-dimensional gridlike structures closely resemble the physical layouts in experimental quantum devices, including those developed by IBM [30]. In Fig. 8, we highlight two such IBM device topologies. Although our results are not tailored to a specific hardware, the structural similarities between our model and these architectures suggest a natural pathway for experimental validation. In particular, the estimation protocol—which relies on spectral and phase information extracted from dynamical observables—can be implemented in IBM's superconducting qubit devices. These platforms support programmable coupling maps and time-resolved measurements, which are essential to realize the phase reconstruction techniques discussed in Ref. [21]. Moreover, IBM's interface allows for fine-grained control over qubit interactions and readout, making them well suited for testing the sensitivity of our protocol to various coupling configurations.

By applying our methods to such architectures, one could investigate which interaction terms are critical for accurate Hamiltonian reconstruction and which can be neglected without significant loss of fidelity. This insight could help develop hardware-aware strategies for calibration, error mitigation, and resource allocation in near-term quantum devices.

ACKNOWLEDGMENT

This work was supported by the Australian Research Council (ARC) Centre of Excellence for Quantum Engineered Systems grant (CE 170100009).

DATA AVAILABILITY

The data that support the findings of this article are not publicly available. The data are available from the authors upon reasonable request.

APPENDIX A: COUPLINGS FOR NEAREST-NEIGHBOR INTERACTION

The tight-binding Hamiltonian in an N-dimensional Hilbert space can be written as

$$H_C = \sum_{n=1}^{N-1} c_n(|n\rangle\langle n+1| + |n+1\rangle\langle n|),$$

where $\{|1\rangle, |2\rangle, \ldots, |N\rangle\}$ are the basis vectors and c_n's are the nearest-neighbor couplings and $c_n > 0$ (see Sec. II) . Let $\{e_k\}$ be the eigenspectrum of H_C and $\langle 1|e_k\rangle$ be the overlap of the kth eigenvector $|e_k\rangle$ with the reference state. We can see that

$$\begin{aligned}\langle 1|H_C &= c_1\langle 2|\\ \Rightarrow \langle 1|H_C|e_k\rangle &= e_k\langle 1|e_k\rangle = c_1\langle 2|e_k\rangle\\ \Rightarrow c_1^2 &= \sum_{k=1}^{N} |e_k\langle 1|e_k\rangle|^2.\end{aligned}$$

Thus, $c_1 = \sqrt{\sum_{k=1}^{N} e_k^2|\langle 1|e_k\rangle|^2}$ and $\langle 2|e_k\rangle = \frac{e_k\langle 1|e_k\rangle}{c_1}$. Once we have c_1, we can recursively calculate the values of c_n, $n = 2, 3, \ldots, N-1$, as shown below:

$$\begin{aligned}\langle n|H_C &= c_n\langle n+1| + c_{n-1}\langle n-1|\\ \Rightarrow \langle n|H_C|e_k\rangle &= e_k\langle n|e_k\rangle = c_n\langle n+1|e_k\rangle + c_{n-1}\langle n-1|e_k\rangle\\ \Rightarrow \langle n+1|e_k\rangle &= \frac{e_k\langle n|e_k\rangle - c_{n-1}\langle n-1|e_k\rangle}{c_n}.\end{aligned}$$

Subsequently,

$$\begin{aligned}c_n\langle n+1|e_k\rangle &= e_k\langle n|e_k\rangle - c_{n-1}\langle n-1|e_k\rangle\\ \Rightarrow \sum_{k=1}^{N} |c_n\langle n+1|e_k\rangle|^2 &= \sum_{k=1}^{N} |e_k\langle n|e_k\rangle - c_{n-1}\langle n-1|e_k\rangle|^2\\ \Rightarrow c_n^2 &= \sum_{k=1}^{N} |e_k\langle n|e_k\rangle - c_{n-1}\langle n-1|e_k\rangle|^2.\end{aligned}$$

Therefore, we conclude that the knowledge of $\langle 1|e_k\rangle$ and e_k is sufficient to compute all the coupling constants.

APPENDIX B: ERROR BOUNDS FOR UP TO $n = 2$

We assume that we already have the values of $\{e_k^\epsilon\}$ and $\{\langle 1|e_k^\epsilon\rangle\}$ and apply the estimation scheme for nearest-neighbor interaction, but substitute $c_n \to c_n^\epsilon$ and $\langle n|e_k\rangle \to \langle n|e_k\rangle_\varepsilon$ to highlight the the possibility that the computed values may diverge from the true values.

For $n = 1$, $(c_1^\epsilon)^2 = \sum_{k=1}^{N}(e_k^\epsilon)^2|\langle 1|e_k^\epsilon\rangle|^2$ and $\langle 2|e_k\rangle_\varepsilon := e_k^\epsilon\langle 1|e_k^\epsilon\rangle/c_1^\epsilon$. The definition for c_1^ϵ does not take into account the terms arising due to the perturbation, resulting in an error in estimating the coupling c_1. Our objective is to find the relation between c_1^ϵ and c_1, as a function of ϵ. Now,

$$\begin{aligned}H^\epsilon|1\rangle &= c_1|2\rangle + \epsilon d_1|3\rangle\\ \Rightarrow \langle 1|(H^\epsilon)^2|1\rangle &= c_1^2 + \epsilon^2 d_1^2\\ \Rightarrow \langle 1|H^\epsilon \sum_{k=1}^{N} |e_k^\epsilon\rangle\langle e_k^\epsilon|H^\epsilon|1\rangle &= c_1^2 + \epsilon^2 d_1^2\\ \Rightarrow \sum_{k=1}^{N} \left(e_k^\epsilon\right)^2 \left|\langle 1|e_k^\epsilon\rangle\right|^2 &= c_1^2 + \epsilon^2 d_1^2\\ \Rightarrow \left(c_1^\epsilon\right)^2 &= c_1^2 + \epsilon^2 d_1^2.\end{aligned}$$

Proceeding in a similar way, we arrive at an expression for $(c_2^\epsilon)^2$, as shown below:

$$\begin{aligned}\left(c_2^\epsilon\right)^2 &= \sum_{k=1}^{N} \left|e_k^\epsilon\langle 2|e_k\rangle_\varepsilon - c_1^\epsilon\langle 1|e_k^\epsilon\rangle\right|^2\\ &= \sum_{k=1}^{N} \left|e_k^\epsilon \frac{e_k^\epsilon\langle 1|e_k^\epsilon\rangle}{c_1^\epsilon} - c_1^\epsilon\langle 1|e_k^\epsilon\rangle\right|^2\\ &= \sum_{k=1}^{N} (e_k^\epsilon)^2 \frac{\left(e_k^\epsilon\right)^2|\langle 1|e_k^\epsilon\rangle|^2}{\left(c_1^\epsilon\right)^2} + \left(c_1^\epsilon\right)^2 \sum_{k=1}^{N} |\langle 1|e_k^\epsilon\rangle|^2\\ &\quad - 2c_1^\epsilon \sum_{k=1}^{N} e_k^\epsilon \frac{e_k^\epsilon|\langle 1|e_k^\epsilon\rangle|^2}{c_1^\epsilon}\\ &= \sum_{k=1}^{N} \frac{\left(e_k^\epsilon\right)^4|\langle 1|e_k^\epsilon\rangle|^2}{\left(c_1^\epsilon\right)^2} + \left(c_1^\epsilon\right)^2 - 2\sum_{k=1}^{N} \left(e_k^\epsilon\right)^2|\langle 1|e_k^\epsilon\rangle|^2.\end{aligned}$$

Setting $(c_1^\epsilon)^2 = c_1^2 + \epsilon^2 d_1^2$ and using $\langle 1|(H^\epsilon)^4|1\rangle = \sum_{k=1}^{N}(e_k^\epsilon)^4|\langle 1|e_k^\epsilon\rangle|^2$, the above equation reduces to

$$\left(c_2^\epsilon\right)^2 = \frac{\langle 1|(H^\epsilon)^4|1\rangle}{\left(c_1^\epsilon\right)^2} - \left(c_1^\epsilon\right)^2.$$

Expanding $(c_1^\epsilon)^2$ and ignoring $\mathcal{O}(\epsilon^3)$, we get

$$\left(c_2^\epsilon\right)^2 = c_2^2 + \epsilon^2\left(d_2 + \frac{d_1 c_3}{c_1}\right)^2 + \mathcal{O}(\epsilon^3).$$

[1] E. Bairey, I. Arad, and N. H. Lindner, Learning a local Hamiltonian from local measurements, Phys. Rev. Lett. **122**, 020504 (2019).

[2] F. Wilde, A. Kshetrimayum, I. Roth, D. Hangleiter, R. Sweke, and J. Eisert, Scalably learning quantum many-body Hamiltonians from dynamical data, arXiv:2209.14328.

[3] D. McNulty, F. B. Maciejewski, and M. Oszmaniec, Estimating quantum Hamiltonians via joint measurements of noisy noncommuting observables, Phys. Rev. Lett. **130**, 100801 (2023).

[4] L. E. de Clercq, R. Oswald, C. Flühmann, B. Keitch, D. Kienzler, H. Y. Lo, M. Marinelli, D. Nadlinger, V. Negnevitsky,

and J. P. Home, Estimation of a general time-dependent Hamiltonian for a single qubit, Nat. Commun. **7**, 11218 (2016).

[5] B. P. Lanyon, C. Maier, M. Holzäpfel, T. Baumgratz, C. Hempel, P. Jurcevic, I. Dhand, A. S. Buyskikh, A. J. Daley, M. Cramer, M. B. Plenio, R. Blatt, and C. F. Roos, Efficient tomography of a quantum many-body system, Nat. Phys. **13**, 1158 (2017).

[6] L. Seveso and M. G. A. Paris, Estimation of general Hamiltonian parameters via controlled energy measurements, Phys. Rev. A **98**, 032114 (2018).

[7] T. Xin, S. Lu, N. Cao, G. Anikeeva, D. Lu, J. Li, G. Long, and B. Zeng, Local-measurement-based quantum state tomography via neural networks, npj Quantum Inf. **5**, 109 (2019).

[8] T. Baumgratz, A. Nüßeler, M. Cramer, and M. B. Plenio, A scalable maximum likelihood method for quantum state tomography, New J. Phys. **15**, 125004 (2013).

[9] S. Xiao, Y. Wang, Q. Yu, J. Zhang, D. Dong, and I. R. Petersen, Quantum state tomography from observable time traces in closed quantum systems, Control Theory Technol. **22**, 222 (2024).

[10] B. Qi, Z. Hou, L. Li, D. Dong, G. Xiang, and G. Guo, Quantum state tomography via linear regression estimation, Sci. Rep. **3**, 3496 (2013).

[11] A. Anshu, S. Arunachalam, T. Kuwahara, and M. Soleimanifar, Sample-efficient learning of interacting quantum systems, Nat. Phys. **17**, 931 (2021).

[12] A. Bakshi, A. Liu, A. Moitra, and E. Tang, Learning quantum Hamiltonians at any temperature in polynomial time, arXiv:2310.02243 (2023).

[13] J. Haah, R. Kothari, and E. Tang, Learning quantum Hamiltonians from high-temperature Gibbs states and real-time evolutions, Nat. Phys. **20**, 1027 (2024).

[14] A. Shabani, M. Mohseni, S. Lloyd, R. L. Kosut, and H. Rabitz, Estimation of many-body quantum Hamiltonians via compressive sensing, Phys. Rev. A **84**, 012107 (2011).

[15] R. Badveli, V. Jagadish, R. Srikanth, and F. Petruccione, Compressed-sensing tomography for qudits in Hilbert spaces of non-power-of-two dimensions, Phys. Rev. A **101**, 062328 (2020).

[16] K. Rudinger and R. Joynt, Compressed sensing for Hamiltonian reconstruction, Phys. Rev. A **92**, 052322 (2015).

[17] S. T. Flammia, D. Gross, Y.-K. Liu, and J. Eisert, Quantum tomography via compressed sensing: Error bounds, sample complexity and efficient estimators, New J. Phys. **14**, 095022 (2012).

[18] D. Burgarth, K. Maruyama, and F. Nori, Coupling strength estimation for spin chains despite restricted access, Phys. Rev. A **79**, 020305(R) (2009).

[19] D. Burgarth and A. Ajoy, Evolution-free Hamiltonian parameter estimation through Zeeman markers, Phys. Rev. Lett. **119**, 030402 (2017).

[20] H. Feng, T.-M. Yan, and Y. Jiang, Applicability of coupling strength estimation for linear chains of restricted access, Chin. Phys. B **29**, 030305 (2020).

[21] D. Burgarth and K. Maruyama, Indirect Hamiltonian identification through a small gateway, New J. Phys. **11**, 103019 (2009).

[22] D. Burgarth and V. Giovannetti, Full control by locally induced relaxation, Phys. Rev. Lett. **99**, 100501 (2007).

[23] F. Barioli, W. Barrett, S. M. Fallat, H. T. Hall, L. Hogben, B. Shader, P. van den Driessche, and H. van der Holst, Zero forcing parameters and minimum rank problems, Linear Algebra Appl. **433**, 401 (2010).

[24] P. Yang, M. Yu, R. Betzholz, C. Arenz, and J. Cai, Complete quantum-state tomography with a local random field, Phys. Rev. Lett. **124**, 010405 (2020).

[25] S.-Y. Hou, H. Li, G.-L. Long, Experimental quantum Hamiltonian identification from measurement time traces, Sci. Bull. **62**, 863 (2017).

[26] J. Zhang and M. Sarovar, Quantum Hamiltonian identification from measurement time traces, Phys. Rev. Lett. **113**, 080401 (2014).

[27] D. Burgarth and K. Yuasa, Quantum system identification, Phys. Rev. Lett. **108**, 080502 (2012).

[28] AIM Minimum Rank–Special Graphs Work Group, Zero forcing sets and the minimum rank of graphs, Linear Algebra Appl. **428**, 1628 (2008).

[29] A. Abdelrahman, O. Khosravani, M. Gessner, A. Buchleitner, H. P. Breuer, D. Gorman, R. Masuda, T. Pruttivarasin, M. Ramm, P. Schindler, and H. Häffner, Local probe of single phonon dynamics in warm ion crystals, Nat. Commun. **8**, 15712 (2017).

[30] A. Kole, S. Hillmich, K. Datta, R. Wille, and I. Sengupta, Improved mapping of quantum circuits to IBM QX architectures, IEEE Trans. Comput. Aided Des. Integr. Circuits Syst. **39**, 2375 (2020).